Hindawi
Journal of Robotics
Volume 2023, Article ID 9827679, 1 page
https://doi.org/10.1155/2023/9827679

Retraction

Retracted: Online Control Method of Small- and Medium-Sized Electromechanical Equipment Based on Deep Neural Network

Journal of Robotics

Received 19 December 2023; Accepted 19 December 2023; Published 20 December 2023

This article has been retracted by Hindawi following an investigation undertaken by the publisher [1]. This investigation has uncovered evidence of one or more of the following indicators of systematic manipulation of the publication process:

(1) Discrepancies in scope
(2) Discrepancies in the description of the research reported
(3) Discrepancies between the availability of data and the research described
(4) Inappropriate citations
(5) Incoherent, meaningless and/or irrelevant content included in the article
(6) Manipulated or compromised peer review

The presence of these indicators undermines our confidence in the integrity of the article's content and we cannot, therefore, vouch for its reliability. Please note that this notice is intended solely to alert readers that the content of this article is unreliable. We have not investigated whether authors were aware of or involved in the systematic manipulation of the publication process.

Wiley and Hindawi regrets that the usual quality checks did not identify these issues before publication and have since put additional measures in place to safeguard research integrity.

We wish to credit our own Research Integrity and Research Publishing teams and anonymous and named external researchers and research integrity experts for contributing to this investigation.

The corresponding author, as the representative of all authors, has been given the opportunity to register their agreement or disagreement to this retraction. We have kept a record of any response received.

References

[1] M. Yang, S. Deng, and Z. Zhao, "Online Control Method of Small- and Medium-Sized Electromechanical Equipment Based on Deep Neural Network," *Journal of Robotics*, vol. 2022, Article ID 1607694, 10 pages, 2022.

Hindawi
Journal of Robotics
Volume 2022, Article ID 1607694, 10 pages
https://doi.org/10.1155/2022/1607694

Research Article

Online Control Method of Small- and Medium-Sized Electromechanical Equipment Based on Deep Neural Network

Mengmeng Yang, Sanxing Deng, and Zhizheng Zhao

College of Mechanical and Electrical Engineering, Huanghe Jiaotong University, Jiao Zuo 454950, China

Correspondence should be addressed to Mengmeng Yang; 2016090903@zjtu.edu.cn

Received 9 August 2022; Revised 15 September 2022; Accepted 21 September 2022; Published 7 October 2022

Academic Editor: Shahid Hussain

In order to improve the online control effect of small- and medium-sized electromechanical equipment, this paper studies the online control method of small- and medium-sized electromechanical equipment combined with the deep audit network. Moreover, starting from the signal basis of online control signal recognition and channel coding recognition of electromechanical equipment, this paper determines the type of online control signal and channel coding type of electromechanical equipment required for the experiment. This paper compares the signals under different types of online control signals for electromechanical devices and clarifies the differences in amplitude, frequency, phase, and spectrum in time-domain waveforms. In addition, through the elaboration of different channel coding theories, this paper clarifies the differences in coding methods. Through the experimental research, it can be seen that the online control effect of the small- and medium-sized electromechanical equipment based on the deep neural network proposed in this paper is very good.

1. Introduction

Different from the conventional monitoring system, the online system applies network technology to the monitoring field and gives full play to the advantages of the existing Internet, which can make the monitoring system have more powerful functions. Users only need to use any computer connected to the Internet to realize remote centralized monitoring and control of the equipment through a common browser [1]. This is of great significance for the informatization and intelligence of the production processes of some enterprises, as well as for some tasks that are not labor-intensive but require long-term supervision, such as mobile phone stations, water gates, and environmental monitoring. In recent years, with the continuous progress of network technology and modern communication technology, the remote monitoring technology based on TCP/IP and B/S mode has gradually matured. It is foreseeable that the application of network technology to monitoring systems will become one of the mainstream directions of remote monitoring technology development in the future [2].

An embedded system is a computer system that is embedded in the object system, centered on the application, can be reduced in software and hardware, and has strict requirements on volume, power consumption, and cost. Compared with the traditional single-chip microcomputer, one of its important breakthroughs is to solve the interconnection problem between the equipment and the Internet, so that people can remotely monitor the equipment of each node in the network through the existing network settings [3]. In recent years, with the rapid development of embedded technology, a wide variety of powerful CPUs and off-chip connections have provided a stable and reliable hardware environment for network applications; embedded operating systems also support this hardware and Ethernet well. The transplantation of the operating system is greatly simplified, which provides convenience for the realization of the embedded remote monitoring system. The embedded remote monitoring system converts the data of various protocols in the monitoring system into a unified TCP/IP protocol format so that users can remotely access the web server through Ethernet to monitor the equipment [4].

Intelligent control is mainly used to solve control complex systems that are difficult to solve by traditional methods. Compared with classical control, its most prominent feature is that the research object is no longer the controlled object, but the controller itself. This feature gives full play to the intelligent characteristics of human beings. Intelligent control is mainly divided into the following categories: (1) Expert control is the most widely used in the field of intelligent control and has been widely used in process control, industrial design, and fault diagnosis. The general expert control system consists of three parts: control mechanism, reasoning mechanism, and knowledge base [5]. (2) Fuzzy control is a kind of control method using fuzzy set theory. Its working process is as follows: first, the information is fuzzified, then the output of fuzzy control is obtained through fuzzy inference rules, and finally, the output of fuzzy control is refined. Calculate the final output control value [6]. (3) Learning control: learning is one of the main bits of intelligence of human beings, and learning control is an attempt to simulate the self-regulation mechanism of human beings. A learning control system is a system that continuously obtains and processes unpredictable information, accumulates experience, and estimates, categorizes, and continuously improves system performance in the work [7]. (4) Neural network control is a relatively new research direction in intelligent control. It is a control method that simulates the activities of the human brain nervous system. Some functions of the system. Neural networks have some characteristics that are particularly suitable for control, such as nonlinear processing capability, parallel processing capability, learning capability, and adaptive capability [8].

In recent years, with the development of intelligent control theory, scholars at home and abroad have applied it to electro-hydraulic servo systems and have carried out a series of studies on the nonlinearity, time-varying parameters, and load transients of electro-hydraulic servo systems. The study in [9] aims at the nonlinearity, time-varying, and model uncertainty of the electro-hydraulic servo system, and the composite synchronous control and fuzzy control are combined to form a fuzzy PID control system. The experimental results show that the controller can improve the dynamic characteristics of the system meaning the control effect is better than the PID control; the literature [10] established a control algorithm that combines multiple groups of PID algorithms and fuzzy PID control algorithms. The fuzzy algorithm is used in the case of large deviations in the system, which can quickly reduce small deviations. The PID algorithm is used in the case of small deviations. Compared with the traditional PID, this control algorithm has a faster dynamic response speed, and the control effect is better when the set pressure changes. Reference [11] aims at the nonlinear effect of the servo system shaking table, based on the traditional PID. The simulation results show that this method can effectively eliminate the output error and can accurately track the given motion trajectory. Reference [12] proposed a direct inverse control method of RBF neural network with a dual network structure, and the controller is controlled according to the system response. The results show that the control strategy can effectively improve the performance of the system, reduce steady-state error, and improve the robustness of the system. In reference [13], aiming at the nonlinear and time-varying hydraulic system, a new type of PID controller based on a neural network is used and simulated by MATLAB software. The simulation results show that the control algorithm can improve the dynamic and static characteristics of the system and has a significant effect.

A networked control system, also known as a networked control system, refers to a control system implemented in a network environment and is divided into a broad networked control system and a narrowly defined networked control system. The network control system in the broad sense includes the network control system in the narrow sense and also includes the monitoring, modulation, and optimization of factory workshops, production lines, and even field equipment through enterprise information networks and Internet/intranet [14]. The narrow network control system refers to the integration of some on-site monitoring, control, and operation equipment and communication lines in a certain area to provide data transmission between equipment, so that equipment and users in different locations in the area can achieve resource sharing and communication. It can also coordinate operations. The network control system is the product of the development and integration of computer technology, communication technology, and control technology. Distributed control systems (DCS), industrial Ethernet, and field bus control systems belong to the network control system in a sense, which reflects the direction of the control system. The development trend of networking, integration, distribution, and node intelligence will be applied in the field of industrial control, building automation, and home automation [15].

From any point of view, the development trend of human-computer interaction reflects the continuous emphasis on the human factor, making human-computer interaction closer to the natural form, enabling users to use daily natural skills without special efforts and learning; cognitive load is reduced, and work efficiency is improved [16]. It can be seen from the development of human-computer interaction technology that the emergence of computers not only brings new problems to human engineering research but also completely changes the guiding ideology of research. Traditional ergonomics regards people as human-machine-environment. The responders and controllers in the system focus on the problem of matching the characteristics and functions of humans and machines at the level of physical motion and regard traditional electromechanical machines as an extension of the human hand [17]. The emergence, development, and widespread popularization of computer technology have enabled machine systems to have a certain level of intelligence, which can partially replace human cognitive functions, so it is regarded as an "extension of the human brain," which requires ergonomics at the level of cognitive theory. This paper examines the cognitive characteristics and functional matching problems of humans and machines [18].

This paper combines the deep neural network to carry out the research on the online control method of small- and medium-sized motor equipment and improves the intelligent effect of online control of small- and medium-sized motor equipment.

2. Basics of Control Identification and Channel Coding Identification of Electromechanical Equipment

2.1. Control Basis of Signal Electromechanical Equipment. The signal electromechanical equipment control can realize the spectrum transfer of the baseband signal. The electromechanical equipment control signal has a stronger anti-interference ability, the signal is safer during the transmission process, and it is convenient for the transceiver and the receiver to synchronize the signal. The control of signal electromechanical equipment is realized by controlling the parameters of the carrier wave, which is usually divided into amplitude modulation, frequency modulation, and phase modulation.

The MASK signal is a modern electromechanical device control signal that uses the carrier envelope amplitude to transmit information. The amplitude of the carrier signal is controlled by the baseband level, which is called a multivariate amplitude shift keying signal. The MASK signal characterizes the M-ary symbol with multiple levels, changing the carrier amplitude through different combinations of binary digits. The MASK signals used in the experiment are 2ASK, 4ASK, and 8ASK signals. The signals can be specifically expressed as

$$s_{\mathrm{MASK}}(t) = Am(t)\cos(2\pi f_c t) = A\left[\sum_n a_n g(t - nT_s)\right]\cos(2\pi f_c t). \quad (1)$$

Among them, A is the basic amplitude, $m(t) = \sum_n a_n g(t - nT_s)$ is the baseband signal that has not been controlled by the electromechanical equipment, a_n is the instantaneous level value of the baseband signal, $g(t)$ is the rectangular pulse signal, T_s is the symbol period, and f_c is the carrier frequency. The value of the symbol a_n can be bipolar, namely, $a_n \in [\pm 1, \pm 3, \ldots]$, or unipolar, namely, $a_n \in [0, 1, \ldots, M-1]$.

Three kinds of MASK signals are used in the experiment, namely 2ASK signal, 4ASK signal, and 8ASK signal. The time-domain signal and spectrum representation of 2ASK electromechanical equipment control are shown in Figure 1.

The time-domain signal and spectrum representation of 4ASK electromechanical equipment control is shown in Figure 2.

The time-domain signal and spectral representation of 8ASK electromechanical device control is shown in Figure 3.

MPSK is a multiphase shift keying control signal for electromechanical equipment, and the baseband signal realizes the control of signal electromechanical equipment by controlling the carrier phase. The MPSK signal is generated by the superposition of M types of carrier signals of the same amplitude and the same frequency with different phases in

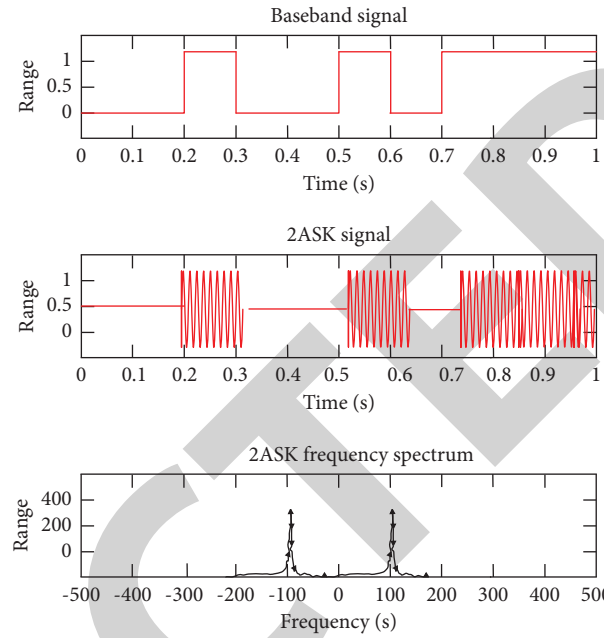

Figure 1: 2ASK time-domain waveform and spectrum.

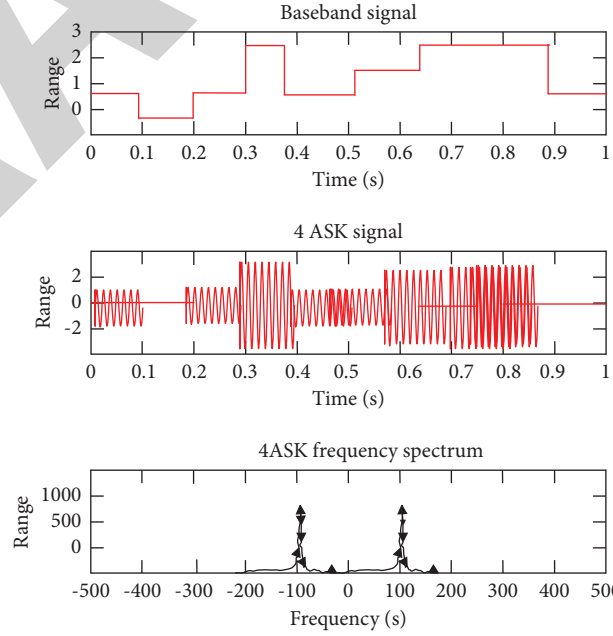

Figure 2: 4ASK time-domain waveform and spectrum.

different time slots, and different phases represent different baseband information. The specific expression of the MPSK signal is

$$s_{\mathrm{MPSK}} = Ag(t)\cos(2\pi f_c t + \theta_n), \ (n-1)T_s \le t \le nT_s. \quad (2)$$

Among them, A is the amplitude factor, $g(t)$ is the rectangular pulse signal, f_c is the carrier frequency, and θ_n is the phase represented by the nth symbol and it has M values. θ_n is generally defined as

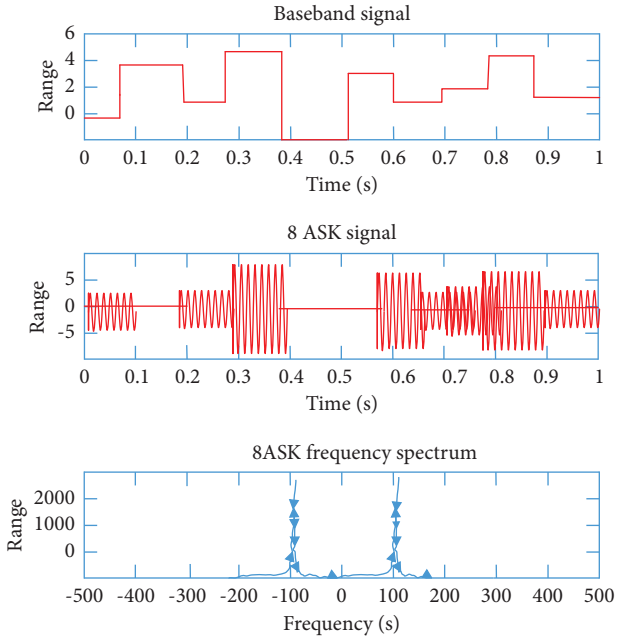

Figure 3: 8ASK time-domain waveform and spectrum.

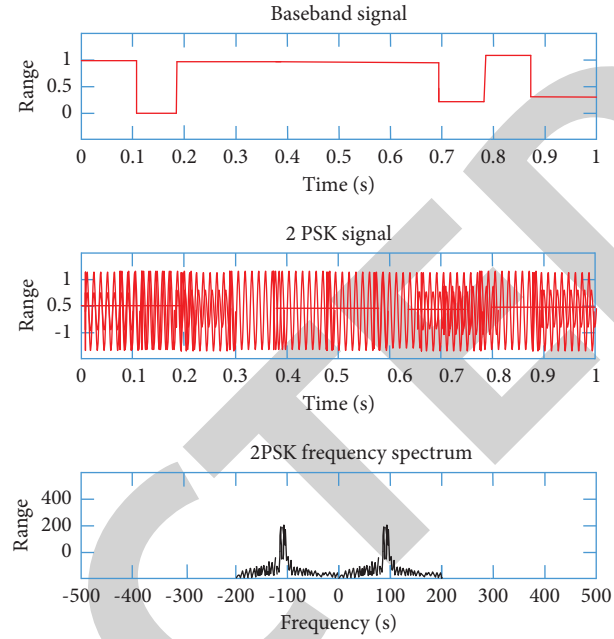

Figure 4: 2PSK time-domain waveform and spectrum.

$$\theta_n = \frac{2\pi i}{M}, \quad i \in [0, 1, \ldots M-1]. \tag{3}$$

The MPSK signal is represented by the in-direction and quadrature components as

$$\begin{aligned} s_{\text{MPSK}} &= Ag(t)\left(\cos\theta_n \cos 2\pi f_c t - \sin\theta_n \sin 2\pi f_c t\right) \\ &= Ag(t)\left(a_{cn}\cos 2\pi f_c t - a_{sn}\sin 2\pi f_c t\right). \end{aligned} \tag{4}$$

There is a one-to-one correspondence between MPSK signal and constellation diagram. According to $a_{cn}^2 + a_{sn}^2 = 1$, it can be known that the constellation diagram of MPSK signal is a circle with a radius of 1.

Three kinds of MPSK signals are used in the experiment, namely, 2PSK signal, 4PSK signal, and 8PSK signal. The time-domain waveform and spectrum of 2PSK signal are shown in Figure 4.

The time-domain waveform and spectrum of the 4PSK signal are shown in Figure 5.

The time-domain waveform and spectrum of the 8PSK signal are shown in Figure 6.

The MFSK signal is a multivariate frequency shift keying signal, and the signal electromechanical equipment control is completed by controlling the frequency of the sinusoidal carrier signal. The amplitude factor of the carrier signal is the same, and the phase is kept continuous. The signals of different carrier frequencies are added in different time slots to obtain the MFSK signal with M element carrier frequency.

$$s_{\text{MFSK}} = Ag(t)\cos\left(2\pi f_n t\right). \tag{5}$$

Among them, A is the basic amplitude factor, $g(t)$ is the rectangular pulse signal, the initial phase of the MFSK signal is generally 0, and f_n is the frequency of the nth symbol and has M kinds of values. Generally, f_n is equally spaced.

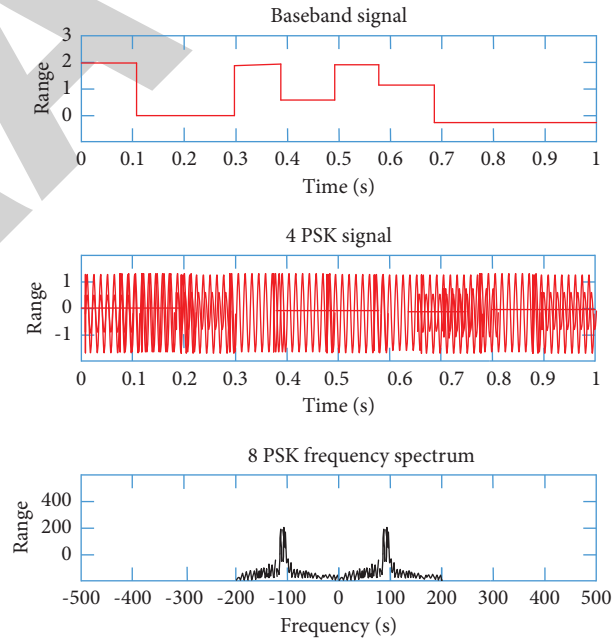

Figure 5: 4PSK time-domain waveform and spectrum.

$$f_n = f_c + \frac{(2i - M + 1)}{2}\Delta f, \quad i = 0, 1, \ldots M-1. \tag{6}$$

f_c is the carrier frequency, Δf is the frequency interval, and if $\Delta f > 0$ is specified, the values of M frequencies can be obtained as $f_c \pm \Delta f/2, f_c \pm 3 \times \Delta f/2, \ldots, f_c \pm (M-1) \times \Delta f/2$ respectively. The carrier frequencies should be as close as possible and intersect each other to reduce the signal bandwidth. The condition of frequency quadrature is that the frequency interval is an integer multiple of $T_s/2$, that is, the minimum frequency interval is $T_s/2$.

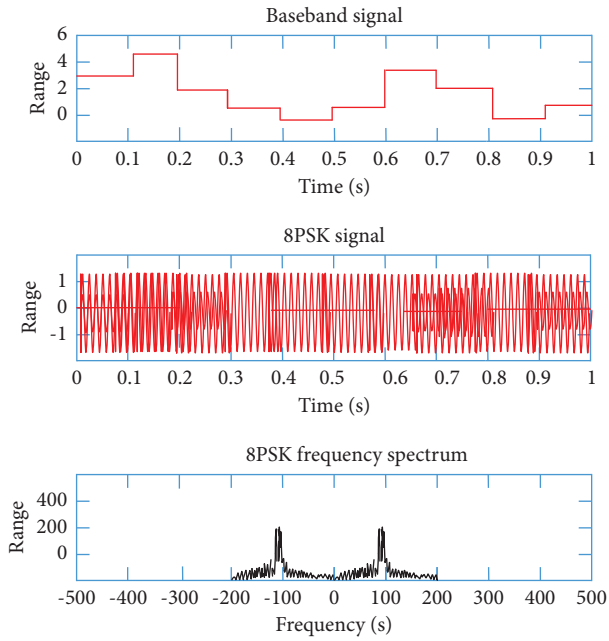

Figure 6: 8PSK time-domain waveform and spectrum.

The MQAM signal is a quadrature amplitude electromechanical device control signal, and the signal amplitude and phase are transformed during the electromechanical device control process. The MQAM signal uses two orthogonal carriers to control the electromechanical equipment of the signal and, at the same time, ensures the noninterference transmission within the bandwidth. The electromechanical device control method of the MQAM signal determines that it has higher stability and stronger anti-interference ability than the above three signals, and the bandwidth utilization rate is also higher. Moreover, it can maintain high electromechanical equipment control efficiency and high frequency band utilization even under the condition of strong noise interference. The expression of the MQAM signal is

$$s_{\mathrm{MQAM}} = Aa_{cn}g(t)\cos(2\pi f_c t) - Aa_{sn}g(t)\sin(2\pi f_c t). \quad (7)$$

Among them, (a_{cn}, a_{sn}) represents the value of the current symbol on the constellation diagram, and each group of values is a signal point, which represents the in-direction component and the quadrature component of the signal.

The constellation diagram of the MQAM signal has two kinds: circular and rectangular. The experiment uses the rectangular constellation diagram to generate an MQAM signal. The circular constellation diagram of MQAM is similar to the MPSK signal, and the synthesized signal amplitude is constant. The MQAM signal generated by the rectangular constellation has a more variable amplitude and can carry both phase information and amplitude information. At the same time, the MQAM signal also maintains a uniform distribution of signal points, which can reduce the bit error rate of signal transmission within a certain range.

Four MQAM signals are used in the experiment, namely, 8QAM, 16QAM, 32QAM, and 64QAM signals. The constellation diagrams of these four signals are shown in Figure 7.

2.2. Channel Coding Basics. Channel coding is a way to ensure the reliable transmission of information. It ensures the reliability of the transmission content through error control, also known as error correction coding. The system judges the received codeword under the condition of known channel coding type and coding parameters. If the redundant elements and information elements of the codeword satisfy the predetermined coding and decoding rules, the codeword is judged to be correct and decoded. In the process of mobile communication development, channel coding types are also constantly updated. The channel coding used in the global mobile communication system in the 2G era is mainly block code and convolutional code. In the 3G era, the use of code division multiple access technology and broadband code division multiple access technology has greatly improved the 3G capacity, and the channel coding technology used has also been updated to Turbo code, which has a performance close to Shannon's limit. In the 4G era, the orthogonal frequency division multiplexing technology and the orthogonal frequency division multiple access technology are mainly used, and the Turbo code is used in the channel coding, but the structure of the Turbo code is optimized to reduce the decoding complexity. With the popularization of 5G mobile communication, channel coding has a wider range of applications, mainly using low-density check codes, polar codes, tail-biting convolutional codes, and turbo codes. This paper mainly introduces five types of coding methods used for experiments, namely, BCH codes, QCLDPC codes, convolutional codes, Turbo codes, and polar codes.

BCH code is a cyclic linear block code, which can correct random errors under the condition of short codes and has high coding performance. The application of the BCH code is relatively mature. In the early days of cellular mobile digital communication, it was often used as an error correction coding method used by base stations and mobile stations. The BCH codes can be divided into two types according to the generator polynomial: one is the original BCH code, and the other is the non-original BCH code.

The symbol of the binary BCH code comes from GF (2), and the original BCH code is introduced here. The generator polynomial $g(x)$ contains the primitive polynomial with the highest degree m, the coding length is $2^m - 1$, the minimum code distance is $\delta = 2t + 1$, and t errors can be corrected in the application process. α represents the primitive element in the field $GF(2^m)$. If the code takes $(\alpha, \alpha^2, \ldots, \alpha^{2t})$ as the root and the minimum polynomial corresponding to each root is $m_i(x)$, $i = 1, 2, \ldots, 2t$, then $g(x)$ can be written as

$$g(x) = \mathrm{LCM}(m_1(x), m_2(x), \ldots, m_{2t}(x)). \quad (8)$$

In the experiment, the BCH code on $GF(2^4)$ is constructed with $t = 2$ and $m = 4$, and the code length is 15. The primitive polynomial of $GF(2^4)$ is $g_0(x) = x^4 + x + 1$. In the

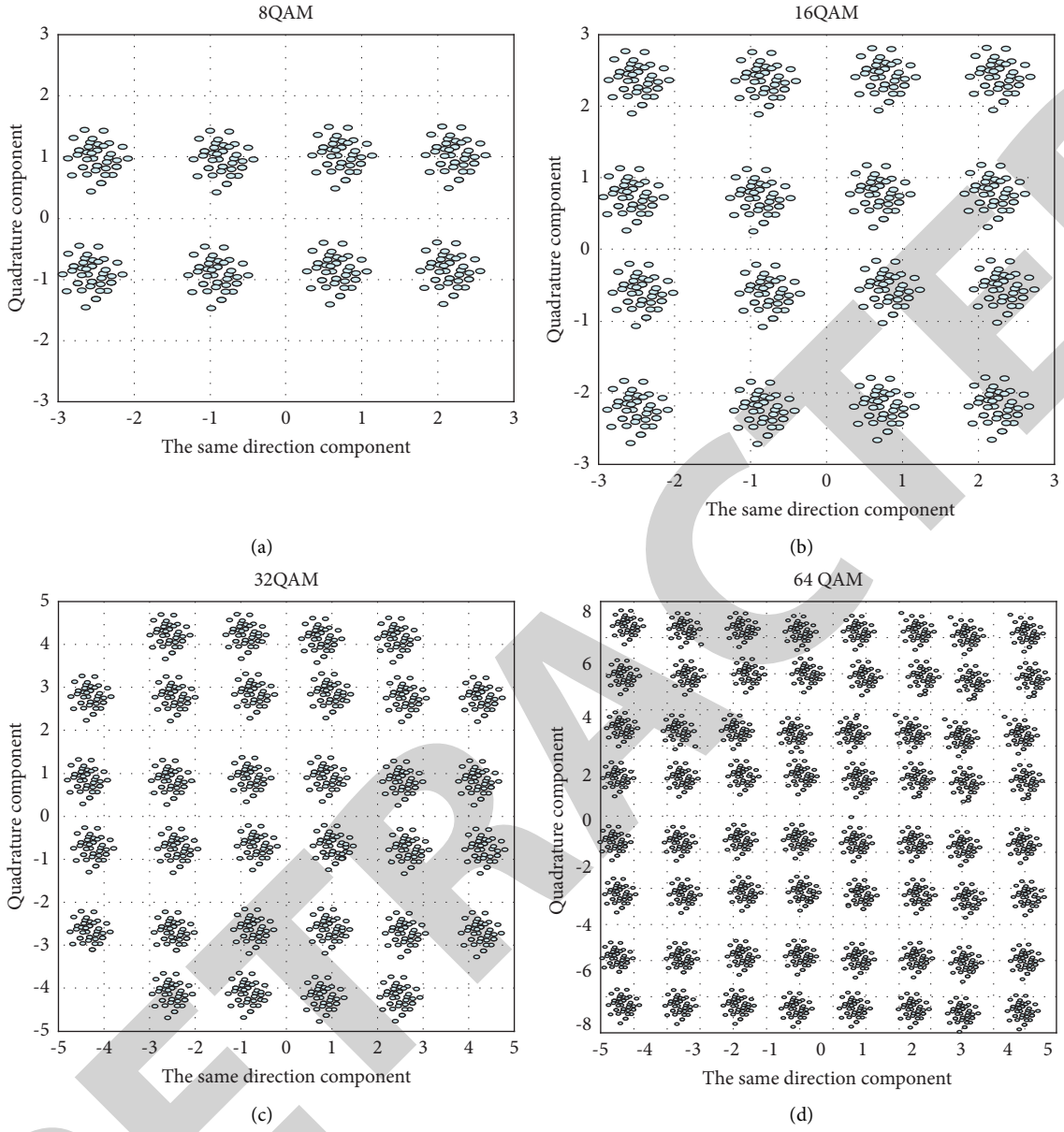

Figure 7: MQAM signal constellation diagram (SNR = 25 dB): (a) 8QAM rectangular constellation diagram; (b) 16QAM rectangular constellation diagram; (c) 32QAM rectangular constellation diagram; (d) 64QAM rectangular constellation diagram.

case of $t = 2$, the BCH code takes α and α^3 as the roots, and the minimum polynomial of α is the minimum polynomial $m_3(x) = x^4 + x^3 + x^2 + x + 1$ of the primitive polynomial $m_1(x) = x^4 + x + 1$, α^3, and the generator polynomial $g(x)$ is obtained as

$$g(x) = m_1(x)m_3(x) = x^8 + x^7 + x^6 + x^4 + 1. \quad (9)$$

Among them, the number of check elements is $m \times t = 8$, which is a (15, 7, 5) BCH code with an error correction capability of 2.

The binary LDPC code is represented by (n, k), the information length is k, and the total length of the codeword is n. It is assumed that m check bits are introduced into the information bit sequence x for coding, a codeword sequence t with a total length of n is generated, and the coding rate is k/n. The encoded codeword t can be represented by an information sequence x and a generator matrix G.

$$t = G^T x. \quad (10)$$

The generator matrix can be written in the form of identity matrix and submatrix

$$G^T = \begin{bmatrix} I_{k\times k} \\ P_{m\times k} \end{bmatrix}. \quad (11)$$

Under the method of hard-decision algebraic decoding, the check matrix H can be expressed as

$$H = [P|I_{m\times m}]. \quad (12)$$

The Tanner graph is a way of describing the parity check matrix of an LDPC code. The nonzero elements in the check matrix correspond to the edges connecting the variable nodes and the check nodes in the Tanner graph, and the number of rows and columns of the check matrix H corresponds to the number of check nodes and the number of variable nodes, respectively. The degree λ of the variable node and the degree γ of the check node in the Tanner graph remain constant, and whether the check matrix H is sparse is judged by the relationship between λ and γ. Figure 8 depicts the parity check matrix H under the condition of $\lambda = 2$ and $\gamma = 3$.

$$H = \begin{bmatrix} 101001 \\ 010011 \\ 001110 \\ 110100 \end{bmatrix}. \tag{13}$$

There are two construction methods for LDPC codes: one is random generation and the other is structured generation. The performance of LDPC codes constructed by the random method is close to the Shannon limit under the condition of long codes, but the decoding is complicated. The code generated by the structure is widely used and has a good effect under the condition of short code, and the coding and decoding algorithm is simple. The most commonly used structured generation method is to use a quasi-cyclic structure to generate codewords. The quasi-cyclic structure can generate a regular check matrix, which greatly simplifies the complexity of the decoding algorithm. At the same time, the quasi-cyclic structure can achieve the purpose of increasing data throughput by reducing the decoding delay and is widely used in practice.

Convolutional code proposes a new block code encoding method, which strengthens the correlation between code groups in the encoding process, and each code group is no longer independent of the other. The codeword output at a certain moment is not only related to the currently input information symbol, but the previous information sequence also affects the current output codeword. Therefore, adding a shift register to the encoder improves the memory of the encoder.

At present, (n, k, m) is commonly used to represent convolutional codes, where n is the length of the codeword, k is the length of the information group, and m is the encoding memory. The more shift registers in the encoder, the longer the information element storage time. N is defined as an encoding constraint. It takes N time slots from the time the information element enters the first shift register until it completely leaves the encoder, and all codewords generated in the N time slots are related to this information element. In addition, the coding constraints represent the number of mutually constrained code groups.$N_A = N \times n$ represents the coding constraint length, N_A is counted in bits, and the number of mutually constrained binary symbols is calculated by using the length of each code group and the coding

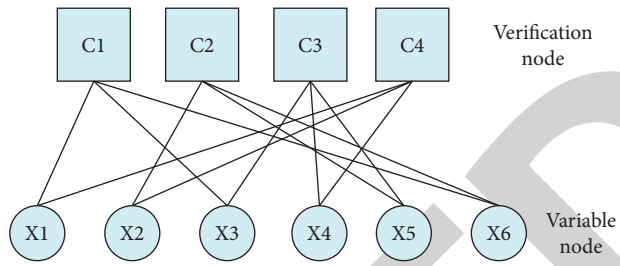

Figure 8: Tanner diagram of the LDPC code under the condition of $\lambda = 2$ and $\gamma = 3$.

constraint. In the actual application process, the encoded information sequence is long, and the complexity of the encoding structure will be greatly improved when the convolutional code encoding memory is long. Therefore, when designing a convolutional code structure, the coding complexity is reduced by reducing the sequence length input to the encoder per unit time.

The experiment adopts (2, 1, 2) convolutional code. The encoder has one input and two outputs. The specific structure is shown in Figure 9. The encoder consists of two shift registers D_1 and D_2, two modulo, two adders, and a switch circuit. If the information elements are sequentially input to the encoder in the order of $m_0 m_1 m_2 \ldots m_{j-2} m_{j-1} m_j \ldots$; the generator polynomial of the output symbols c_{j1} and c_{j2} is

$$\begin{cases} c_{j1} = m_j + m_{j-2} \\ c_{j2} = m_j + m_{j-1} + m_{j-2} \end{cases}. \tag{14}$$

The generated sequence is

$$g^{(1)} = (101), g^{(2)} = (111). \tag{15}$$

The information sequence is $u = (u_0, u_1, \ldots)$, the two output sequences of the encoder are $c^{(1)} = (c_0^{(1)}, c_1^{(1)}, c_2^{(1)}, \ldots)$ and $c^{(2)} = (c_0^{(2)}, c_1^{(2)}, c_2^{(2)}, \ldots)$, and the output sequence is formed by the convolution of the input symbols through the two impulse responses of $g^{(1)}$ and $g^{(2)}$. If the impulse response lasts at most N time units, $N = \mathrm{m} + 1$, then

$$g^{(1)} = \left(g_0^{(1)}, g_1^{(1)}, \ldots, g_m^{(1)}\right), g^{(2)} = \left(g_0^{(2)}, g_1^{(2)}, \ldots, g_m^{(2)}\right). \tag{16}$$

The encoded output sequence can be written as

$$\begin{cases} c^{(1)} = u * g^{(1)} \\ c^{(2)} = u * g^{(2)} \end{cases}. \tag{17}$$

The encoding process is expressed as a generator matrix as

$$c = uG. \tag{18}$$

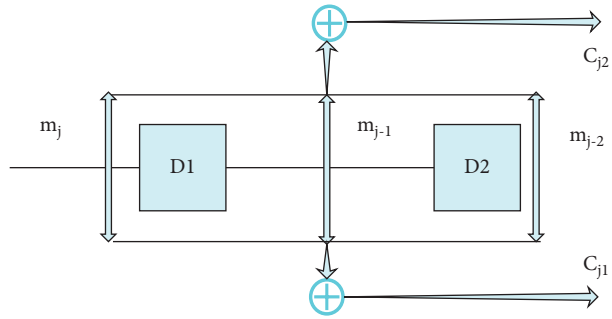

Figure 9: Encoder with (2, 1, 2) convolutional code.

Among them, the generating matrix is

$$G = \begin{bmatrix} g_0^{(1)}g_0^{(2)} & g_1^{(1)}g_1^{(2)} & g_2^{(1)}g_2^{(2)} & \cdots & g_m^{(1)}g_m^{(2)} \\ g_0^{(1)}g_0^{(2)} & g_1^{(1)}g_1^{(2)} & \cdots & g_{m-1}^{(1)}g_{m-1}^{(2)} & g_m^{(1)}g_m^{(2)} \\ g_0^{(1)}g_0^{(2)} & \cdots & g_{m-2}^{(1)}g_{m-2}^{(2)} & g_{m-1}^{(1)}g_{m-1}^{(2)} & g_m^{(1)}g_m^{(2)} \\ \ddots & \ddots & & & \end{bmatrix}. \quad (19)$$

The information element sequence M of length k is input into the encoder, and the buffer adds n-k bits to the information sequence to obtain the code group C_0. C_0 is input into the interleaver and the recursive systematic convolution (RSC) coding unit in parallel and is input into another RSC coding unit through one way of the interleaver to obtain C_1 and C_2, respectively. C_0, C_1, and C_2 are cascaded in parallel, and the codeword C is obtained by puncturing and multiplexing the structure. The code length of the Turbo code used in the experiment is $n = 24$, the information bit length is $k = 12$, the code rate is $k/n = 1/2$, and pseudo-random interleaving is used.

The information transmission process can also be equivalent to the transmission process in two channels, the high-performance channel transmits information bits, and the low-performance channel transmits frozen bits.

The code length is $N = 2^n$, $n \geq 0$, and for a given N, the codeword x_1^N is generated by $x_1^N = u_1^N G_N$, where u_1^N is the information sequence and G_N is the generator matrix of $N \times N$. The bit channel index set is $I = \{1, 2, \ldots N\}$, and A is a subset of the index set I; then, the codeword generation can be rewritten as

$$x_1^N = uG_N(A) \oplus u_c G_N(A^c). \quad (20)$$

Among them, $A^c = \{1, 2, \ldots, N\} - A$ is the complement of A, and $G_N(A)$ is the sub-matrix of G_N, which is composed of row vectors whose elements in set A are numbered as G_N and $u = \{u_i, i \in A\}$.

If the information sequence u is the bit to be transmitted, and the fixed set is A, the resulting code is called the coset code of G_N. A G_N coset code is determined by the parameter (N, K, A, u_c), $K = |A|$ is the information bit length of the code, K/N is the code rate, A is the information set, and u_c is the frozen bit. For example, the codeword determined by $(4, 2, \{2, 4\}, (1, 0))$ can be expressed as

$$x_1^4 = u_1^4 G_4 = (u_2, u_4)\begin{bmatrix} 1010 \\ 1111 \end{bmatrix} + (1, 0)\begin{bmatrix} 1000 \\ 1100 \end{bmatrix}. \quad (21)$$

When the information sequence is $(u_2, u_4) = (1, 1)$, the corresponding codeword is $x_1^4 = (1, 1, 0, 1)$.

The main problem of polar code construction is how to choose the information set A, which is usually based on the metric parameters to sort the bit channel reliability. The metric parameter used in the experiment is the channel capacity. The metric parameters of the channel are calculated and arranged in order of size, and the bit channel with the larger parameter is selected as the information bit index.

The experiment uses a polar code coding structure with $N = 8$ and a code rate of $R = 1/2$. The polarized channel is shown in Figure 10. The metric parameters of each channel are calculated and sorted.

According to the sorting result, it is clear that the pointer of the information bit points to (U_4, U_6, U_7, U_8) and the remaining channels transmit frozen bits.

3. Online Control Method of Small and Medium Electromechanical Equipment Based on Deep Neural Network

The second part of the algorithm is used as the equipment online signal processing algorithm. Figure 11 shows the structure diagram of the BP neural network PID control.

The controller consists of two parts. The classical PID controller performs closed control on the controlled object, and the entire control system constitutes a closed-loop feedback control structure. The neural network performs autonomous learning and online adjustment of the three key parameters kp, ki, and kd in the PID controller. Moreover, combined with the real-time data of the operation of the control system, it automatically obtains the combined parameters that can make the control performance of the PID controller achieve the best and realizes the optimization of the final performance index.

The online control effect of the small- and medium-sized electromechanical equipment in this paper is evaluated, the quantitative processing of the control effect is carried out with multiple groups of simulations, and the results shown in Table 1 are obtained.

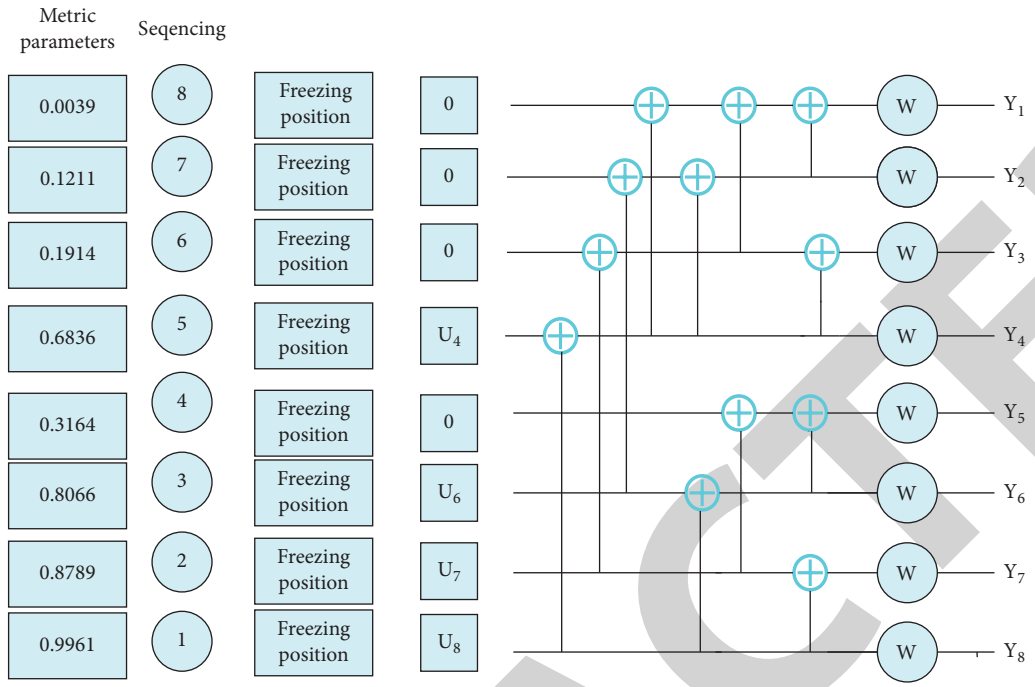

Figure 10: Polarization channel and structure of polar codes.

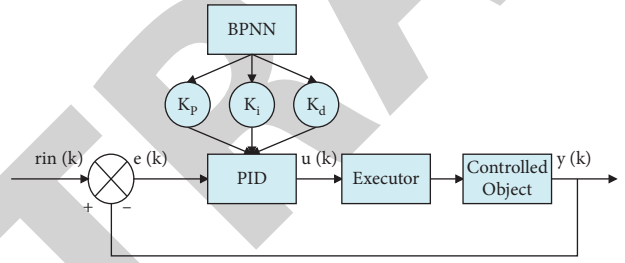

Figure 11: Control diagram of electromechanical equipment based on neural network.

Table 1: Online control effect of small- and medium-sized electromechanical equipment.

Number	Online control	Number	Online control	Number	Online control
1	91.25	17	90.16	33	90.02
2	92.98	18	89.87	34	90.52
3	92.05	19	92.26	35	89.10
4	90.72	20	92.33	36	91.95
5	89.01	21	89.35	37	93.96
6	91.62	22	90.11	38	93.65
7	93.12	23	90.98	39	93.59
8	91.61	24	90.94	40	90.75
9	92.82	25	92.24	41	89.23
10	90.82	26	93.37	42	89.07
11	93.62	27	92.48	43	91.31
12	89.89	28	89.20	44	91.13
13	91.36	29	93.78	45	92.21
14	93.30	30	93.11	46	93.36
15	91.99	31	92.37	47	92.76
16	93.29	32	93.08	48	89.32

It can be seen from the above research that the online control effect of small- and medium-sized electromechanical equipment based on deep neural network proposed in this paper is very good.

4. Conclusion

With the expansion of the production scale of production enterprises and the improvement of flexible production levels, more and more production enterprises hope to realize the networking of production equipment and establish a production monitoring system. An embedded remote monitoring system is the product of the combination of network and industrial equipment measurement and control mechanisms. It connects the measuring mechanism and the control mechanism distributed in the electromechanical equipment through the on-site control network and the Internet, realizes the remote information exchange between the user and the electromechanical equipment, and completes the remote monitoring and control. For small- and medium-sized electromechanical equipment, there are obvious signal problems in online control. This paper combines the deep audit network to research the online control method of small- and medium-sized motor equipment and improve the intelligent effect of online control of small- and medium-sized motor equipment. Through the experimental research, it can be seen that the online control effect of the small- and medium-sized electromechanical equipment based on the deep neural network proposed in this paper is very good.

Data Availability

The labeled datasets used to support the findings of this study are available from the corresponding author upon request.

Conflicts of Interest

The authors declare no conflicts of interest.

Acknowledgments

This work was supported by Huanghe Jiaotong University.

References

[1] Y. Bichiou and H. A. Rakha, "Developing an optimal intersection control system for automated connected vehicles," *IEEE Transactions on Intelligent Transportation Systems*, vol. 20, no. 5, pp. 1908–1916, 2019.

[2] H. Chen, B. Jiang, and N. Lu, "A multi-mode incipient sensor fault detection and diagnosis method for electrical traction systems," *International Journal of Control, Automation and Systems*, vol. 16, no. 4, pp. 1783–1793, 2018.

[3] M. Dumitrescu, "Marine industry automation systems simulation," *Scientific Bulletin "Mircea cel Batran" Naval Academy*, vol. 22, no. 2, pp. 7–13, 2019.

[4] K. Eltag, M. S. Aslamx, and R. Ullah, "Dynamic stability enhancement using fuzzy PID control technology for power system," *International Journal of Control, Automation and Systems*, vol. 17, no. 1, pp. 234–242, 2019.

[5] S. J. Gambhire, D. R. Kishore, P. S. Londhe, and S. N. Pawar, "Review of sliding mode based control techniques for control system applications," *International Journal of dynamics and control*, vol. 9, no. 1, pp. 363–378, 2021.

[6] C. Gehrmann and M. Gunnarsson, "A digital twin based industrial automation and control system security architecture," *IEEE Transactions on Industrial Informatics*, vol. 16, no. 1, pp. 669–680, 2020.

[7] M. S. Jansi and M. K. Elaiyarani, "Iot based home automation system," *Turkish Journal of Computer and Mathematics Education (TURCOMAT)*, vol. 11, no. 3, pp. 2246–2253, 2020.

[8] O. V. Kryukov, I. V. Gulyaev, and D. Y. Teplukhov, "Method for stabilizing the operation of synchronous machines using a virtual load sensor," *Russian Electrical Engineering*, vol. 90, no. 7, pp. 473–478, 2019.

[9] W. Liang, M. Zheng, J. Zhang et al., "WIA-FA and its applications to digital factory: a wireless network solution for factory automation," *Proceedings of the IEEE*, vol. 107, no. 6, pp. 1053–1073, 2019.

[10] B. Pratap and S. Purwar, "Real-time implementation of nonlinear state and disturbance observer-based controller for twin rotor control system," *International Journal of Automation and Control*, vol. 13, no. 4, pp. 469–497, 2019.

[11] M. Saraswat, K. Sharma, N. R. Chauhan, and R. K. Shukla, "Role of automation in energy management and distribution," *Journal of Scientific and Industrial Research (JSIR)*, vol. 79, no. 10, pp. 951–954, 2020.

[12] T. A. Skouras, P. K. Gkonis, C. N. Ilias, P. T. Trakadas, E. G. Tsampasis, and T. V. Zahariadis, "Electrical vehicles: current state of the art, future challenges, and perspectives," *Cleanroom Technology*, vol. 2, no. 1, pp. 1–16, 2019.

[13] K. Wang, E. Tian, J. Liu, L. Wei, and D. Yue, "Resilient control of networked control systems under deception attacks: a memory-event-triggered communication scheme," *International Journal of Robust and Nonlinear Control*, vol. 30, no. 4, pp. 1534–1548, 2020.

[14] C. Wei, M. Benosman, and T. Kim, "Online parameter identification for state of power prediction of lithium-ion batteries in electric vehicles using extremum seeking," *International Journal of Control, Automation and Systems*, vol. 17, no. 11, pp. 2906–2916, 2019.

[15] D. Xu, B. Wang, G. Zhang, G. Wang, and Y. Yu, "A review of sensorless control methods for AC motor drives," *CES Transactions on electrical machines and systems*, vol. 2, no. 1, pp. 104–115, 2018.

[16] Y. Yuan, H. Yuan, D. W. C. Ho, and L. Guo, "Resilient control of wireless networked control system under denial-of-service attacks: a cross-layer design approach," *IEEE Transactions on Cybernetics*, vol. 50, no. 1, pp. 48–60, 2020.

[17] M. Zhang, Y. Zhang, and X. Cheng, "An enhanced coupling PD with sliding mode control method for underactuated double-pendulum overhead crane systems," *International Journal of Control, Automation and Systems*, vol. 17, no. 6, pp. 1579–1588, 2019.

[18] S. Zinchenko, V. Mateichuk, P. Nosov et al., "Use of simulator equipment for the development and testing of vessel control systems," *Electrical, Control and Communication Engineering*, vol. 16, no. 2, pp. 58–64, 2020.